This is a peer-reviewed, author's accepted manuscript of the following research article:
Hu, F., Lu, H., Xu, G., Lv, L., Chen, L., & Shao, Z. (2022).
Carbon quantum dots improve the mechanical behavior of polyvinyl alcohol/polyethylene glycol hydrogel.
Journal of Applied Polymer Science, 139(34), [e52805]. https://doi.org/10.1002/app.52805

Carbon quantum dots improve the mechanical behavior of polyvinyl alcohol/polyethylene glycol hydrogel

Feng Hu [a], Hailin Lu [a, b, *], Guangshen Xu [a], Leifeng Lv [c, *], Lu Chen [a] and Zhonglei Shao [d, *]

[a] Group of mechanical and biomedical engineering, Xi'an key laboratory of modern intelligent textile equipment, College of Mechanical & Electronic Engineering, Xi'an Polytechnic University, Xi'an, Shaanxi 710048, P.R. China.

[b] Taizhou Medical New&Hi-tech industrial Development Zone, Kouan Street, Gaogang District, Taizhou, Jiangsu 225321, P. R. China.

[c] Department of Orthopedics, The Second Affiliated Hospital of Xi'an Jiaotong University, Xi'an Jiaotong University, Xi'an, Shaanxi 710061, P.R. China.

[d] Faculty of Engineering, University of Strathclyde, Royal College, 204 George Street, Glasgow G1 1XW, United Kingdom.

*Corresponding authors.

E-mail addresses: lu@xpu.edu.cn (Hailin Lu), 15529351957@163.com (Leifeng Lv), zhonglei.shao@strath.ac.uk (Zhonglei Shao)

Abstract

As the wear and tear effects of artificial joints disturb patients after joint replacement, techniques of new lubrication materials or methods are constantly being investigated. Hydrothermal method was adopted to produce carbon quantum dots (CDs), and physically cross-linked polyvinyl alcohol-polyethylene glycol hydrogel (PVA-PEG) to encapsulate CDs, which was evaluated as a lubricant for lubrication appraisal with their slow-release solution. Results of the friction experiment showed that the addition of CDs changed the structure of the gel and promoted the tribological properties of the gel. The structural characterization results show that the CDs are successfully wrapped in gel. The network cross-link structure of the gel is improved due to the addition of CDs, which are shown by the results of thermogravimetric analysis (TGA) and differential scanning calorimetry analysis (DSC). At the same time, CDs can influence the thermal stability and crystallinity of the gel as well as the degree of cross-linking. These results of TGA and DSC suggest that the curled molecular chain will not be stretched during the gel cross-linking process. After 2 hours of self-healing, the recovered gel did not break again under the pull of external force. All these contribute to the preparation and application of hydrogels which is worth looking forward to accelerate the development of polymer lubrication.

Key words: polyvinyl alcohol (PVA); carbon quantum dots (CDs); polyethylene glycol (PEG); tribological; self-healing.

1 Introduction

Artificial joint replacement is regarded as an effective means when people have abnormal joints. It is estimated in 2010 that the number of individuals with joint replacement in the USA corresponds to 7.2 million, and it is showing a rising trend in future.[1] Total hip replacement (THR) is regarded as a successful operation with relatively few comorbidities.[2,3] However, the wear of joints is a major problem for failure modes in artificial joints, and corrosion of the materials used in artificial joints may lead to implant failure.[4,5] In the application of artificial joints, friction debris will be generated due to the existence of friction and wear, which can induce macrophages to secrete osteolytic factors to cause osteolysis, and then lead to aseptic loosening, which is one of the main reasons for the failure of artificial joints.[6] Nowadays some researchers are adding lubricants into an artificial joint to achieve great tribological properties.[7-9]

In the replacement of artificial joints, longer service life can be achieved with better materials and thus contribute to the lifetime of the artificial joint.[10,11] There has been excellent progress in the study of combining cobalt-chromium-molybdenum (CoCrMo) alloy with ultrahigh molecular weight polyethylene (UHMWPE) as a material used for joint replacement.[12] However, the wear of the material limits the application of artificial joints.[13] In the UHMWPE/CoCrMo alloy artificial joint pairing, UHMWPE is a less hard material, tends to wear more easily.[14] Therefore, it is worthwhile to investigate the improvement of the frictional properties of two materials, CoCrMo alloy and UHMWPE as artificial joints.[15,16] Adding lubricant would be a common method, but the complex environment of the human body causes the liquid lubricant to be absorbed or explained carefully, thus the service interval of lubricant would be reduced significantly.[17] Therefore one way to provide long-term lubrication to the artificial joint became important.

Hydrogels are polymers bonded by intermolecular hydrogen bonding forces and have many applications in repairing soft tissues, filling tissue cavities, and delivering drugs.[18-20] The special three-dimensional structure of hydrogels gives them excellent water locking properties.[21] The biocompatibility of polyvinyl alcohol (PVA) and polyethylene glycol (PEG) in gel systems enable them to be used in a wide range of applications.[22] Chen et al.[23] has prepared a PVA-HA/PAA compound hydrogel that has a favorable thermal stability and an excellent lubricating property by freeze-thawing and annealing methods. Gang et al.[24] obtained composite hydrogels with nano-hydroxy apatite (HA) nanoparticles filled in polyvinyl alcohol hydrogel (PVA-H) and investigated its lubrication properties. Carbon dots (CDs) are a kind of spherical carbon particles. Compared to metallic quantum dot materials, CDs are almost non-toxic.[25] Because of their small size, they can fill the pores between the contacting materials and thus improve the frictional properties between the materials and have favorable lubrication effects.[26,27] Guo et al.[28] implemented slow-release lubrication with CDs and thermosensitive poly(epsilon-caprolactone)-poly(ethylene glycol)-poly(epsilon-caprolactone) (PCL-PEG-PCL, PCEC) hydrogel. The results show that the composite PCEC/CDs hydrogel release solution has the ability to reduce the friction coefficient significantly.

In this work, my team prepared CDs using chitosan (CS) through the hydrothermal method. PVA was used to cross-link with PEG, and it was desired to encapsulate the CDs in the cross-linked hydrogel, the CDs are then released to provide a medium for better lubrication. XPS, XRD, Raman, FT-IR, TGA, and DSC were used to characterize the PVA/PEG/CDs hydrogels prepared in this article. The lubrication effect of hydrogel was also studied using a GSR-2 friction machine to compare the coefficients of friction (COF) of UHMWPE/CoCrMo alloy contacts. Finally, the mechanism of CDs promoting gel lubrication and mechanical performance was discussed. The research results provide an effective method for improving the life cycle of liquid lubricants. In addition, the positive properties of the gel show potential for a large range of applications in artificial joints or other biological tissues.

2 Experimental

2.1 Materials

Polyvinyl alcohol (PVA, average molecular weight: 25000-30000 Da) and polyethylene glycol (PEG, average molecular weight: 3600-4000 Da) were purchased from Tianjin Damao Chemical Reagent Factory (Tianjin, China). The glacial acetic acid was purchased from Tian in Fuyu Fine Chemical (Tianjin, China). The Chitosan (CS, degree of deacetylation ≥90.0%, molecular weight, 700000–800000 Da) was purchased

from Shanghai Lanji Technology (Shanghai, China). The materials used in this study were of analytic reagent (AR) grade.

2.2 Samples preparation

The Carbon Dots (CDs) were prepared through the hydrothermal method.[29,30] First of all, glacial acetic acid (1 g) was dissolution in distilled water (99 mL) to obtain 1% glacial acetic acid solution. And then, CS 200 mg was added to 20 mL 1% glacial acetic acid solution, after dissolving at 60 ℃ until the solution is clear. Then, let the mixture solution was placed on heating furnace at 130 ℃ for 10-15 hours. After that, the mixture was cool to room temperature. Finally, the supernatant of the mixture was centrifuged at 4000 rpm and filtered to obtain a CDs solution (0.8 wt.%). In the preparation process described in Figure 1, the CDs solution shows a light-yellow color in natural light, however, the purple light (wavelength: 365 nm, power: 20 W) irradiation shows a light-blue color. This may be contributed by the different emission wells on the surface of the CDs. PEG solutions with varying concentrations (10, 20, 30, 40 and 50 wt.%) were prepared by adding different weights of PEG powder to different volumes of distilled water. Obtained PEG solutions with varying concentrations are then added into CDs for PEG/CDs sol. Pour 10g of PVA into the beaker, then add 90 mL of distilled water, heat and dissolve to obtain a PVA solution (10 wt.%). PVA solution and PEG solution and PEG/CDs sol were mixed in 1:1 volume ratio and centrifuged for 5 min to obtain PVA-PEG and PVA-PEG/CDs gel.

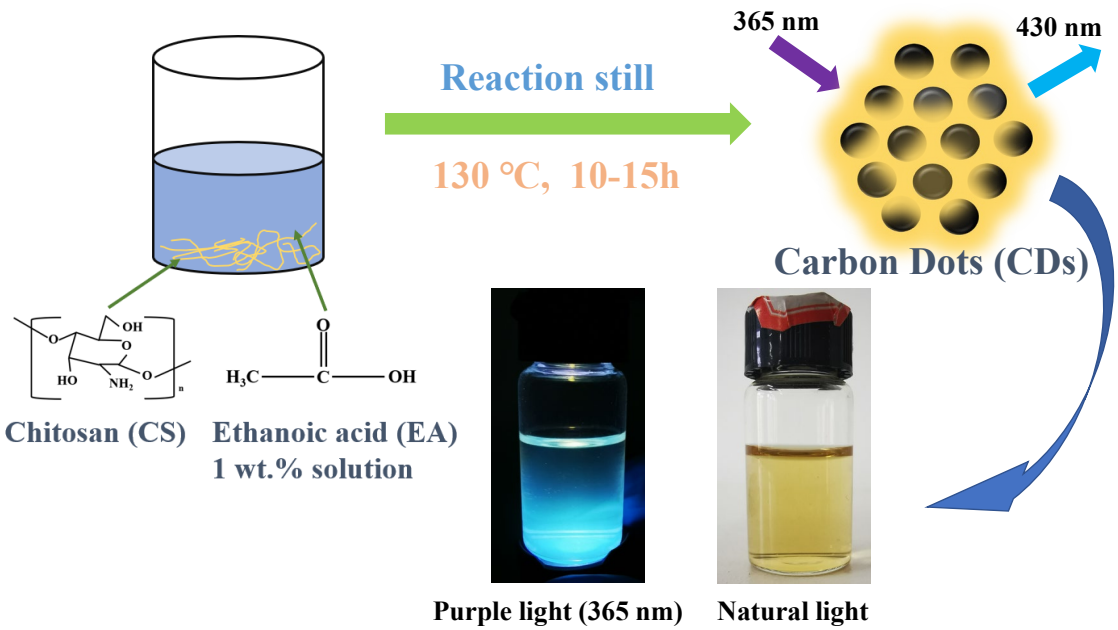

Fig. 1 Schematic diagram of CDs preparation flowchart.

2.3 Friction experiment

The tribological properties were investigated using the GSR-2 friction machine (Rubber alcohol friction testing machine, Shenzhen Zhijia Instrument Equipment Co., Ltd, China). The friction pair is a UHMWPE ball (diameter: 9.525 ±0.05 mm) and CoCrMo (diameter: 30 ±0.1 mm) alloy disk, because of the importance of UHMWPE and CoCrMo as materials of artificial joint parts. The samples were made to slide against a disk with a reciprocation drive system at room temperature (25-30 °C). Before each test, the UHMWPE ball and CoCrMo alloy disk

were swabbed with water and acetone for 10 to 15 seconds and then allowed to dry. In the friction test, the water solution is first introduced between the friction pairs to correct the frictional force data. Then after testing the frictional forces of different materials as lubricants. The frictional forces are measured by a high-performance force sensor (DY054-A, Bengbu Dayang Sensing System Engineering Co., Ltd, China), which provides an accuracy of ±0.006. The accuracy of the experimental platform was adjusted so that the absolute value of positive and negative frictional forces collected by the sensor in the reciprocating motion of the friction testing machine was the same. Frictional forces measurements are made at room temperature and relative temperature at the humidity of 20-30 %. The applied load range was 2-10 N, and each friction experiment lasted 30 minutes. The experiment was repeated three times and the results were averaged for analysis. The COF is calculated by using the frictional force value obtained. Equation (1) for calculating COF is given below, where F_1 is the data measured by the sensor and F_2 is the applied load.

$$COF = \frac{F_1}{F_1} \qquad (1)$$

2.4 Characterization

The prepared gels were dried in a vacuum (relative vacuum pressure: -100 KPa) oven at 60 ℃ for 5-7 days so that the water was completely evaporated, and then powder samples were used for characterization. The D8 advanced diffractometer (Bruck, Germany) was used to characterize the crystal structure of the gel by X-ray diffraction (XRD). This is a method for determining the phase present in the material and can be used to analyze whether CDs are present in the prepared gel. The Escalab 250XI X-ray photoelectron spectrometer (XPS) was used to analyze the elemental composition of the material (Thermo Fisher Scientific, USA). It is often used as a structural analysis, from the results it is possible to infer the structure of the substances contained in the gel sample. The Raman measurements were performed using Horiba Jobin Yvon (Model Hr800, USA), with an excitation wavelength of 514 nm laser. The experimental conditions were as follows: 17 mW liquid output, 600 grating, objective ×10, time 10 s, wave number 500 to 3500 cm^{-1}. The analysis of Raman spectrum can infer the vibration and rotation energy level of the material, and then the prepared gel can be identified and analyzed according to the Raman characteristic shift peak. The specific interactions were studied using Fourier transform infrared spectroscopy (FT-IR). The samples were scanned with a Nicolet IS50 spectrometer (Thermo Fisher Scientific, USA) at wavelengths ranging from 500 cm^{-1} to 4000 cm^{-1}. This test can be used to analyze the molecular structure and chemical composition of substances, and then infer the types of functional groups contained in the gel, and then determine its molecular chemical structure. Thermogravimetric (TGA) and differential scanning calorimetry (DSC) analyses were performed by using the 409C thermobalance (NETZSCH Group, Germany) at temperatures ranging from 30 to 800 °C (heating rate: 0.16 °C/s) in an oxygenated atmosphere. On the one hand, these two tests can know the change of the weight of the sample with the increase of temperature, and on the other hand, it can know which of the sample is endothermic and exothermic. Further, the stability of the gel can be inferred from this result.

2.5 Experiment method

The contact angle was measured using the labeling method. About 15 μL of solution was dropped onto the surface of the CoCrMo disk using a syringe containing solutions PEG and PEG/CDs. Subsequently, a photograph was taken horizontally in the direction of the disk. The contact angle between the droplet and the surface of the disk in the resulting photograph was measured to obtain the contact angle data. The surface

hardness was tested using a shore durometer (Shanghai Precision Instrument Co., Ltd, China). The hydrogels were placed in the molds, and the hydrogel samples were obtained after the cross-linking was completed. After that, excess water was removed from the hydrogel surface and the instrument was been slowly pressed into the hydrogels in vertical direction. The hardness data is obtained from the digital display until the measuring head of the instrument is fully inserted into the hydrogel.

2.6 Biological tests

The PVA, PVA-PEG, and PVA-PEG/CDs three group hydrogel after drying has been cut powder that enough small, and then use high temperature autoclaving to sterilize. The component of cell medium: 10 % Gibco (Vokawi (Beijing) Biotechnology Co., LTD, Beijing, China), 100 U/mL penicillin-100 μg/mL streptomycin and RPMI1640 (Gibco). The third generation L929 cell recovery has been used biocompatibility test. Waiting for the cell to grow about 80 % (Nanoantek Automated Cell Counter ADAM-MC2, Aventur International Trade (Shanghai) Co., Ltd, Shanghai, China), discard medium and use bio-clean PBS solution wash twice. Pancreatin (Gibco) was added to digestion for 1 min after that resuspend and centrifugated. The supernatant was discarded and joined cell medium to cell sediment to obtain cell suspension. The cell suspension has been mixed and counted, cell density about 1, 000 in one hole on 96-well plates. One well pours into a cell medium about 150 μL. In the state of 37 ℃ and 5 % CO_2 box grow cell for 12 hours. Each group joins 10 mg materials and which have six compound holes. Discard materials and medium after 24 hours, use bio-clean PBS solution wash twice, each hole pour 10 μL CCK8 medium solution. Waiting for 1 hour and low-speed oscillation in shake for 10 min to obtain balance solution. The OD value of each well at 450 nm was measured using a microplate reader (FLUOstar Omega), and the measured data was recorded and plotted as a visualization graph.

3. Results and Discussion

3.1 Analysis of XPS and XRD

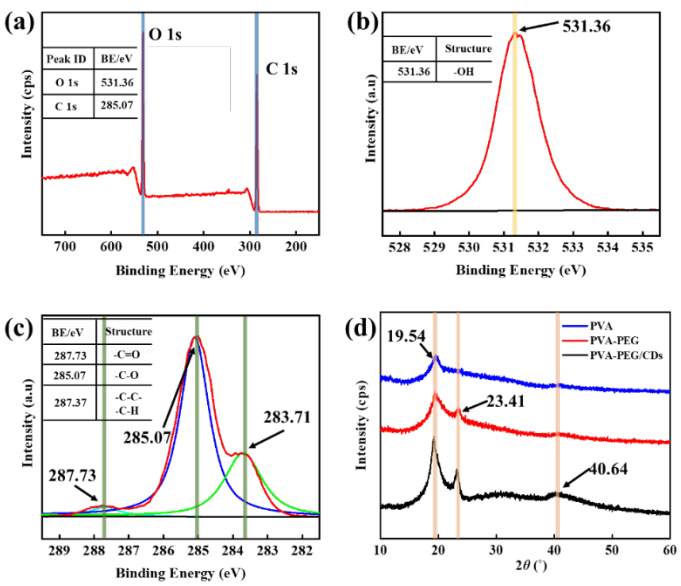

Fig. 2 The XPS spectra patterns of PVA-PEG/CDs; (a) XPS characterizations; (b) XPS O 1s spectrum and (c) XPS C 1s spectrum; (d) The XRD patterns of PVA, PVA-PEG and PVA-PEG/CDs.

The XPS analysis of the hydrogel PVA-PEG/CDs is shown in Fig.2. As is shown in Fig. 2a, the high-resolution XPS characterization has been drawn. The maximum peaks located at 285.07 and 531.36 are attributable to the carbon (C) and oxygen (O) atoms, respectively. The enlarged view of the O 1s spectrum was depicted in Fig. 2b. The peak at 531.36 has been attributed to the presence of the hydroxyl group.[31] Additionally, the C 1s spectrum in Fig. 2c were plotted using Gaussian deconvolution. Among them, the maxima at 287.73, 285.07, and 283.71 can be attributed to -C=O, -C-O-, and -C-C-/-C-H, respectively.[32] Furthermore, the XRD patterns of the three materials were shown. In the sample PVA, the peak point located at 2θ=19.54° is typical of the PVA peak.[33] While in the sample PVA-PEG, the added peak was located at 2θ=23.41°. This can be considered to be contributed by the addition of PEG.[34] In addition, the new maximum in the sample PVA-PEG/CDs located at 2θ=40.64° can be considered to be contributed by CDs.[35] In conclusion, these characterizations elaborate the composition of PVA-PEG/CDs hydrogels and substances contained.

3.2 Analysis of Raman, FT-IR and TGA, DSC

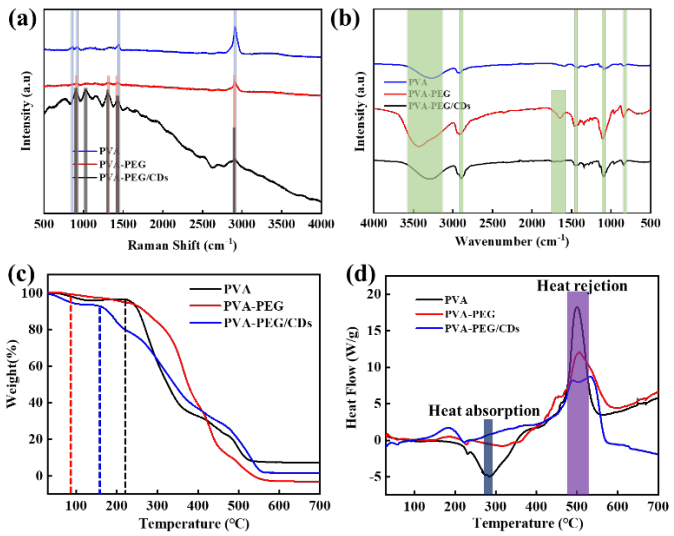

Fig. 3 Raman, FT-IR and TGA, DSC spectra of PVA, PVA-PEG and PVA-PEG/CDs; (a) Raman patterns; (b) FT-IR spectra; (c) TGA curves; (d) DSC curve.

Table1 Raman Peak Summary

PVA absorb peak (cm^{-1})	PVA-PEG absorb peak (cm^{-1})	PVA-PEG/CDs absorb peak (cm^{-1})
2916.04	2906.14	2906.12
1438.85	1429.42	1429.42
924.44	1316.96	1307.53
858.42	915.01	1027.47
		905.58

Table2 FT-IR Peak Summary

PVA absorb peak (cm^{-1})	PVA-PEG absorb peak (cm^{-1})	PVA-PEG/CDs absorb peak (cm^{-1})
3603.81-3057.92	3682.93-3067.68	3630.71-3077.11
2946.51-2879.04	2963.20-2820.97	2963.21-2808.67
1412.73	1635.47	1716.72
1084.78	1462.06	1467.14-1403.29
833.02	1103.65	1092.04
	838.10	835.19

Are shown in the Fig. 3a, the Raman patterns of PVA, PVA-PEG and PVA-PEG/CDs can be seen. For sample PVA Raman patterns, there are four absorption peaks at 2916.04 cm^{-1}, 1438.85 cm^{-1}, 924.44 cm^{-1} and 858.42 cm^{-1}, respectively.[36] While after cross-linking with PEG, the

Raman patterns for sample PVA-PEG shifted to absorption peaks located at 2906.14 cm^{-1}, 1429.42 cm^{-1}, 1316.96 cm^{-1} and 915.01 cm^{-1}, respectively. It can be traced back to the cross-linking effect of the hydrogel, which caused a Raman shift of the sample.[37] The new peak at 1316.96 cm^{-1} can be attributed to the Raman characteristic peak of carbon atom. Compared with PVA, it may be caused by the C-C contained in the newly added PEG.[38] In contrast, the Raman patterns of the samples PVA-PEG/CDs after cross-linking of PVA with PEG/CDs were located at 2906.12 cm^{-1}, 1429.42 cm^{-1}, 1307.53 cm^{-1}, 1027.47 cm^{-1} and 905.58 cm^{-1}, respectively. It is noteworthy that a new peak located at 1027.47 cm^{-1} was also able to be observed along with the generation of Raman shifts. It can be attributed to the addition of CDs, which caused the shift in the Raman spectrum.[39] Fig. 3b shows the FT-IR spectra of the three samples. The main signal was observed at 3100-3400 cm^{-1}, which can be traced to the presence of hydroxyl groups [40]. And the absorption peaks in the FT-IR spectra at 2916 cm^{-1}, 1639 cm^{-1}, 1458 cm^{-1} and 1104 cm^{-1} are associated with the stretching of C-H, C=O, C=C, and C-O bonds, respectively. The other peaks at 800-900 cm^{-1} can be attributed to the bending of C-C and CH_2.[40,41] While the disappearance of the peak located around 1639 cm^{-1} evident in the PVA-PEG/CDs gel sample can be attributed to the reduction of the C=C bond.[42,43] There is an agglomeration effect between CDs and PEG molecules and this behavior affects the presence of the C=C bond, leading to the disappearance of the peak. TGA and DSC was used to determine the thermal properties of PVA, PVA-PEG and PVA-PEG/CDs. Fig. 3c demonstrates the TGA behavior of three samples. TGA curves showed that PVA was stable up to 248 °C, after that initial weight loss. At last, the PVA stop weight loss occurs above the 512 °C and finally weight only 8 % of the starting. The reason is that the PVA melting due to temperature rise caused weight loss. The temperature of the weight loss after PVA cross-link PEG was larger than pure PVA. This is attributed not only to the structure of hydrogel but also the intermolecular hydrogen bonding by polymer cross-link.[44] In contrast, the gel of PVA cross-link PEG inclusion CDs exerts lower heat stability. This is likely due to the presence of CDs that will affect the construction of PVA-PEG gel. Some intermolecular hydrogen construction deformation results from CDs intervene. This makes the heat stability of PVA-PEG/CDs gel lower. The results of three samples DSC analysis were presented in Fig. 3d. For pure PVA, significant heat absorption and exothermic peak can be observed. PVA cross-linked with PEG shows a significant disappearance of the heat absorption peak located around 290 °C. This is because the lattice state changes after cross-linking and the heat absorption required for the melting of PVA was missing. In contrast to pure PVA or PVA-PEG hydrogels, the addition of CDs significantly modified the heat absorption process of the hydrogels, and there is no longer an obvious heat absorption peak. Moreover, the exothermic peak located at 508 °C was also decreased compared to that of pure PVA. Further, the exothermic peak of PVA-PEG/CDs gels was also decreased, which was due to the addition of CDs filling the gel structure, resulting in a lower combustion exotherm. In conclusion, TGA and DSC indicate that the addition of CDs reduces the thermal stability of PVA-PEG gels, which implies that PVA-PEG/CDs gels may contain deeper potential in terms of thermal controlled slow-release.

3.3 The lubrication effect of PEG solution and PEG/CDs sol

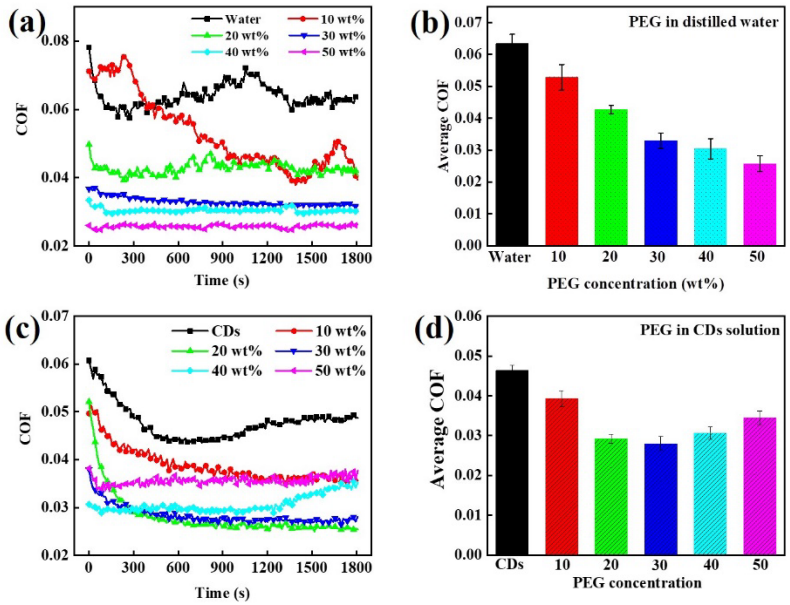

Fig. 4 (a)Transient variation of COF and (b) Variation of the average COF for PEG concentrations in distilled water; (c) Transient variation of COF and (d) Variation of the average COF with PEG concentration in CDs solution.

PEG solution has excellent lubricating properties, showing varying lubrication performance at different concentrations of PEG. Fig. 4a depicts the COF transient curve for varying PEG concentrations. Obviously in the low PEG concentration state, the COF changes significantly in a short time. In contrast, the COF curve for the higher concentration of PEG solution shows that the curve tends to be stable. It is because PEG provides a lubricating effect due to the formation of transfer film. Transfer film formation at low PEG concentration conditions appears to be slower, while at high PEG concentration conditions the transfer film formation appears to be faster. The reason for that results in a stable COF transient variation at high PEG concentrations. Fig. 4b shows the average COF values for the 6 kinds of solutions and it can be observed that the average COF values show a tendency to decrease with increasing PEG concentration. This implies that if PEG is used as a lubricating substance, the higher the concentration of PEG in the solution within a certain range, the more obvious the lubricating effect will be. Noticeable differences in the lubrication effect appear when CDs are added to the PEG solution. Fig. 4c depicts a plot of the transient COF curve displayed by the addition of varying PEG to the CDs solution. Compared with the PEG solution without the addition of CDs, the general trend of transient varying COF runs from high to low, after which there is a slowly increasing trend. It can be attributed to the fact that the addition of CDs changed the lubrication mode of a single PEG as a lubricant. CDs as a small-scale molecule enables PEG molecules to encapsulate CDs. To further cause agglomeration of PEG molecules, which leads to higher COF transient values in the early stage. With the friction experiment, the agglomerated CDs and PEG molecules gradually unfolded and the transfer film was formed gradually. The reason led to a decreasing trend of transient COF. Then, the CDs molecules gradually break the transfer film, which increases the interlayer shear force. It makes the transient COF show a slowly increasing trend. The average COF of different PEG concentrations in the CDs solution is shown in Fig. 4d. The CDs enhanced PEG lubrication effect is limited, with the best performance reached PEG concentration of 30 wt.%. Their average COF is only 0.028. This is attributed to the agglomeration phenomenon of PEG molecules in CDs solution. When the PEG concentration becomes too dense, the

agglomerated PEG molecules hinder the shear force in the frictional pairing movement. In conclusion, the agglomeration of PEG molecules in CDs at appropriate PEG concentration contributes to the lubrication performance, which attributes to the promotion of the PEG lubrication effect by CDs.

3.4 The analysis of contact angle

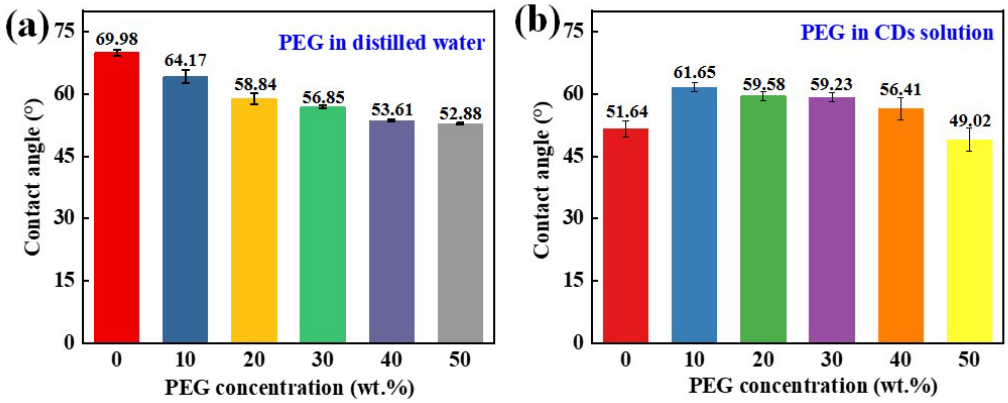

Fig. 5 The contact angle of diffident solution on CoCrMo alloy disk; (a) PEG in distilled water and (b) PEG in CDs solution.

The intermolecular force of the PEG solution was speculated by measuring the static contact angel on CoCrMo alloy disk, and the value as show in Fig. 5a. These dates suggest that the contact angle of PEG solution displayed a curvilinear increase with advancing PEG concentration in distilled water. This could be attributed to the total weight of PEG solution dripping on the CoCrMo alloy disk increasing significantly due to the concentration progress. The change occurs in Fig. 5b, where the contact angle of the PEG/CDs solution on the CoCrMo alloy disk decreases less significantly with increasing PEG concentration. It is noteworthy that the contact angle of the pure CDs solution on the CoCrMo alloy disk is only 49.5 °. In contrast, the contact angles measured for PEG dissolved in distilled water versus solutions containing CDs, respectively, are not the same. This implies that PEG becomes entangled with CDs. Although the PEG concentration increased, the intermolecular forces increased after entanglement. This resulted in a greater contact angle on the CoCrMo alloy disk for PEG in the solution containing CDs at the same concentration conditions. This result suggests that PEG can interact with certain groups of CDs molecules, implying that the polymer PEG can encapsulate CDs. However, there is no significant difference in the value gap, which means that CDs molecules are likely to interact with hydroxyl groups.

3.5 The lubrication effect of PVA-PEG/CDs hydrogel

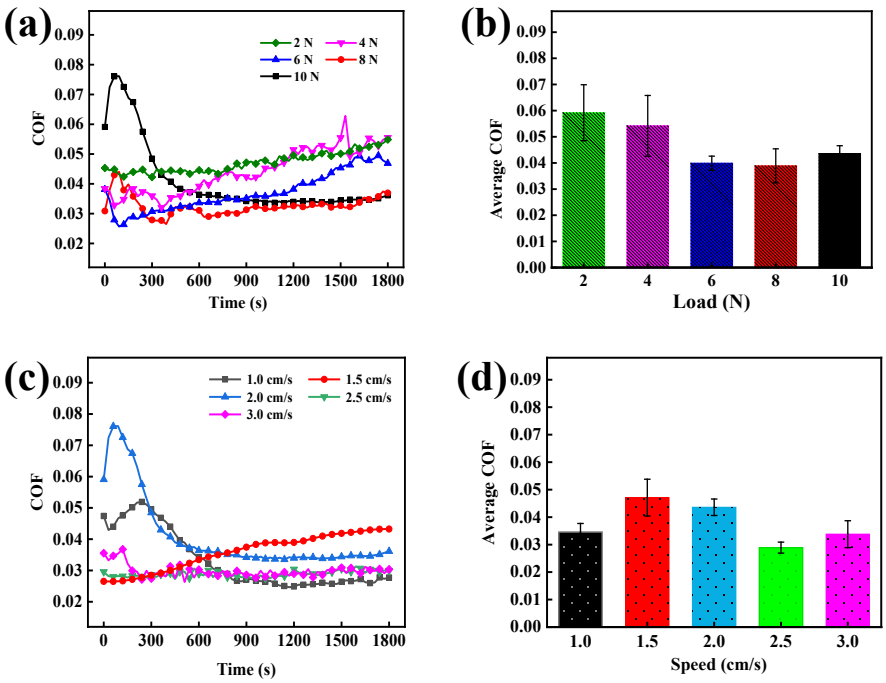

Fig. 6 (a) Transient variation of COF and (b) Variation of the average COF with different load; (c) Transient variation of COF and (d) Variation of the average COF with different speed.

PVA (10 wt.%)-PEG (30 wt.%)/CDs (0.8 wt%) hydrogel as lubricants were investigated in different loads and speeds. As shown in Fig. 6a, the COF of hydrogel was a report in the condition of five groups load and certain speed (2.0 cm/s). Among them, all the transient COF shows a lower value at the experiment start and a higher value at the experiment end. In contrast, few higher load groups transient variation COF shows higher value in test start. This can attribute to the hydrogel structural failure for high pressure on the contact surface. In Fig. 6b, the average COF of five groups load was described. The trend of COF value shows decreases firstly and then increases. This means that the hydrogel can withstand a limited amount of pressure. The reason is possibly caused by hydrogel intermolecular hydrogen bonding is a weak force, which can be easily destroyed under the action of external load. The COF of hydrogel was investigated in the state of five group speed and certain load (10 N) as shown in Fig. 6c. Transient variation of COF has not been observed distinct fluctuation with speed increase. This is likely due to that though the hydrogel intermolecular hydrogen bonding is a weak force, the speed is hard to destroy. The contact surface pressure provided for speed changing is limited. Five groups speed average COF was reported in the state of the hydrogel as lubricants as shown in Fig. 6d. At 2.5 cm/s, the COF of hydrogel dropped to the lowest value. This means that hydrogel as lubricants have a certain range of application. Higher speed may cause hydrogel release lubricating material have not into friction interface. Both of load and speed experiment report the hydrogel lubrication effect, which provides a reference for the performance of a hydrogel.

3.6 The performances of mechanics

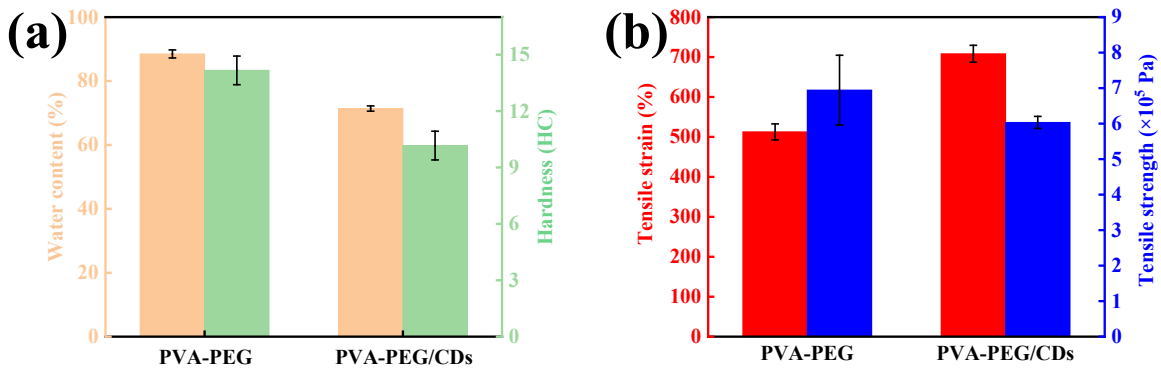

Fig. 7 (a) Water content and hardness of PVA-PEG and PVA-PEG/CDs hydrogel; (b) Tensile strain and strength of PVA-PEG and PVA-PEG/CDs hydrogel.

The water content and hardness results summarized in Fig. 7a show a decreased value in both performances with the addition of CDs. Compared to the PVA-PEG hydrogel, the water content decreased significantly from 88.5 % to 71.5 % with the addition of CDs. Of note, concomitantly, surface hardness performances also were lowered from 14 HC to 9.5 HC in that test. This is most likely to be because the addition of CDs leads to PVA molecule occur crimp behavior, which decreases the action of hydrogen contacts further affect the cross-linked degree. At the same time, for the max tensile strain rate there was an increase in the trend observed as shown in Fig. 7b. It is worth noting that the max tensile strength value can be observed a remarkable decrease. This can be attributed to the fact that PVA molecule occurs crimp leads to cross-linked degree reduction. Which not only effects tensile performances but also changed in mechanics behavior. The results show that the carbon dots can enhance the mechanical properties of the PVA-PEG hydrogel, and the maximum tensile deformation is significantly enhanced.

3.7 The self-healing of PVA-PEG/CDs gel

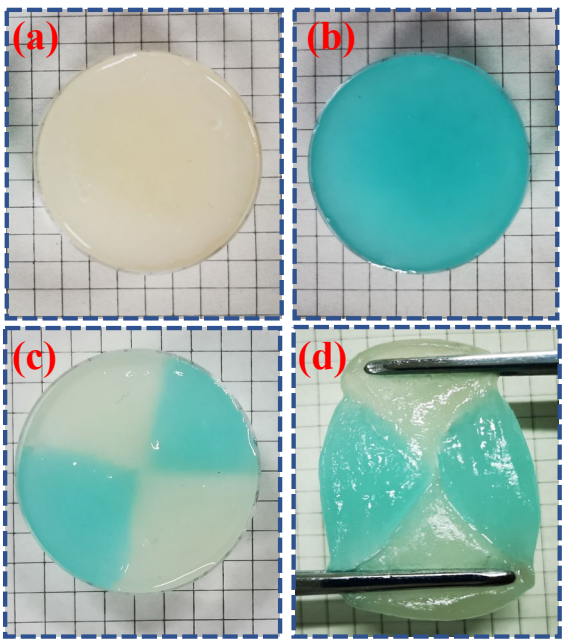

Fig. 8 (a) PVA-PEG/CDs hydrogel; (b) PVA-PEG/CDs hydrogel with methylene blue staining; (c) Two kinds hydrogel splicing; (d) Hydrogel be stretched after self-healing.

There are two kinds of PVA-PEG/CDs hydrogel which are nature color (Fig. 8a) and methylene blue staining (Fig. 8b). The hydrogel without added methylene blue appears light yellow under natural light, and the dyeing effect of methylene blue makes the gel added with it appear light blue. After that, a part of each of the two hydrogels was spliced to observe the self-healing process. As shown in Fig. 8c, the spliced gel was immersed in a 30wt.% PEG solution. Due to the presence of methylene blue, the boundary of the contact site is visible. Two hours after the self-healing process took place, the hydrogel was taken out and subjected to an external force tensile test. The self-healing process of the gel progressed without being broken by an external force, as shown in Fig. 8d. The process of self-healing reveals that there are hydrogen bonds between the hydrogels, and can self-heal without relying on external forces in the case of disconnection. This is because although the gel is cut, there are bare hydroxyl groups at the wound. Later, when it comes into contact with another part of the gel containing hydroxyl groups, the cross-linking reaction occurs again, showing self-healing behavior.

3.8 The swelling rate and biocompatibility

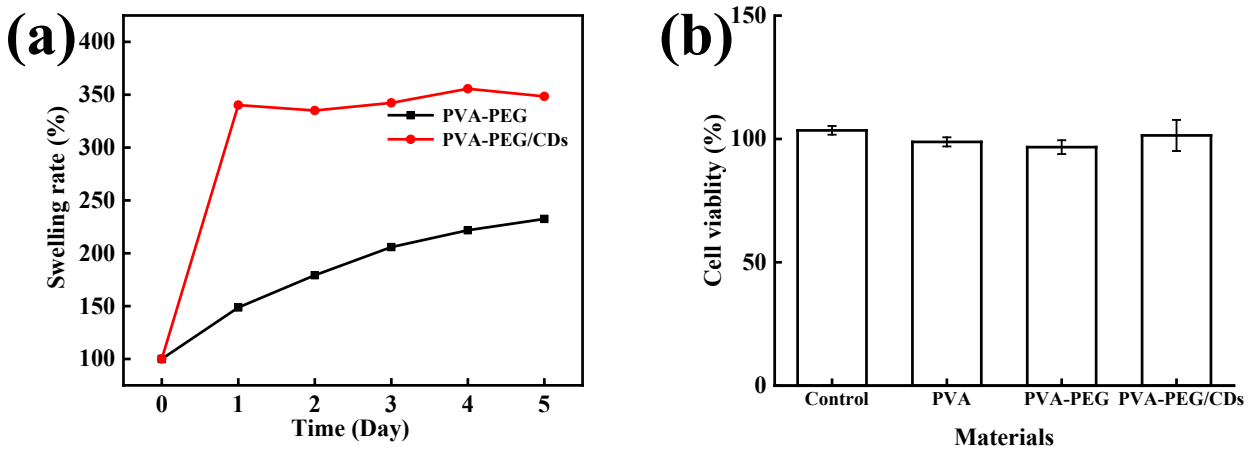

Fig. 9 (a) Swelling rate of PVA-PEG and PVA-PEG/CDs hydrogel; (b) Cell viability by MTT.

The swelling behavior of the hydrogel was tested with or without the addition of CDs, as shown in Fig. 9a. The swelling behavior of PVA-PEG hydrogel without added CDs showed a slow increase trend and finally stopped at about 230% of the initial weight. This indicates that the swelling and water absorption of the hydrogel can be expanded to about twice its weight. In contrast, the swelling behavior of PVA-PEG hydrogels with CDs seems to reach saturation on the first day. As the number of days increased, water absorption did not occur. Furthermore, the swelling behavior brought the final weight of the hydrogel to about 3 times the initial weight. This can be attributed to the fact that the addition of CDs affected the molecules of the cross-linked hydrogel, causing it to curl. After dehydration, it swells by absorbing water again, and the curled molecules are more easily stretched, thereby absorbing more water. Fig. 9b shows the absorbance value (OD value) measured by enzyme-linked immunoassay at 540 nm. This value is expressed in the change in cell proliferation rate relative to the control group. It can be concluded that cell growth is almost uninhabited. The cell proliferation rate of PVA, PVA-PEG, and PVA-PEG/CDs gel is close to that of the control group. This result proves the biocompatibility of PVA-PEG/CDs gel.

3.9 The mechanism analysis

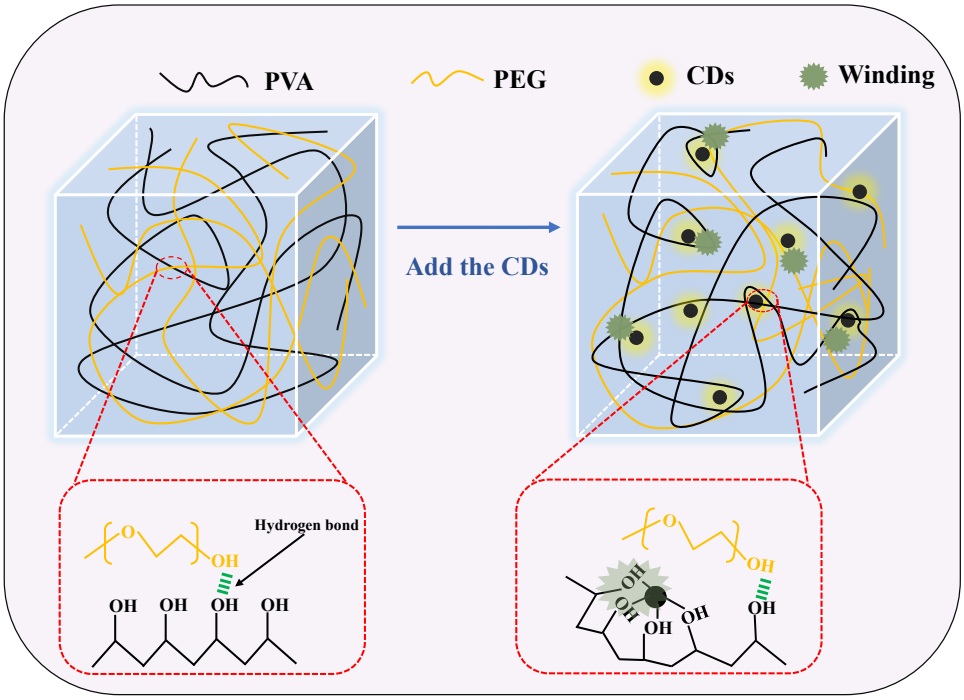

Fig. 10 Mechanism diagram of CDs acting on PVA-PEG/CDs hydrogel.

As shown in Fig. 10, the polymer substance in the gel forms a hydrogel under the action of the hydrogen bonding force, which has a pore structure and a three-dimensional network. Among them, the cross-linking of polyvinyl alcohol and polyethylene glycol is accomplished through these effects. After adding CDs, the attractive surface of this molecule can adsorb groups such as hydroxyl groups. This causes the PVA molecule to produce a curling behavior, which causes a decrease in the degree of crosslinking. In addition, the FT-IR characterization results showed that the gel after the addition of CDs showed a phenomenon that the strength of the hydroxyl group decreased. At the same time, the DSC results also showed that the crystallinity of PVA-PEG/CDs hydrogel decreased. These are all due to the reduction in the number of hydroxyl groups that the polymer can contact with each other, which reduces the hydrogen bonding necessary to form a gel. These common results lead to more release of PEG during the friction process. Correspondingly, the curled molecules in the gel are pulled apart during the stretching process, showing a strong tensile deformation rate.

4 Conclusions

In this article, using CS as a carbon source, CDs were prepared by hydrothermal method, and CDs were mixed with PEG, and then cross-linked with PVA to explore the tribological properties and mechanics of the gel with the addition of CDs. The results showed that the addition of CDs changed the cross-linking process of the gel. Friction experiments show that the added gel has better tribological properties and is also enhanced in terms of mechanics. Although the tensile strength has decreased, the tensile deformation rate has increased. The mechanism of action is that certain groups contained on the surface of CDs molecules can be entangled with PVA molecules, which reduces the tensile strength after cross-linking. Subsequently, the PVA molecules are gradually unfolded as the stretching progress, which exhibits a higher rate of tensile deformation. The friction experiment also complements this point. When a part of the lubricant PEG is released under pressure, more lubricant can be released due to the existence of entanglement, thereby improving the lubricating performance of the gel. In addition, biocompatibility

experiments show that the gel is safe to use. With the development and application of gels, CDs can change the effect of gels with great potential exploration value.

Acknowledgments

This work was supported by Xi'an Key Laboratory of Modern Intelligent Textile Equipment (No.2019220614SYS021CG043), Ph.D. research startup foundation of Xi'an Polytechnic University (No.107020516).

Author Contributions

Feng Hu and Hailin Lu developed the initial concept. Feng Hu and Hailin Lu wrote the initial paper. Lu Chen assisted with data acquisition and data analysis. Leifeng Lv provides data for biological evaluation. All authors discussed the results and commented on the manuscript.

Conflict of Interest

The authors declare that they have no known competing financial interests or personal relationships that could have appeared to influence the work reported in this paper.

References

1. Kremers, H. M.; Larson, D. R.; Crowson, C. S.; Kremers, W. K.; Washington, R. E.; Steiner, C. A.; Jiranek, W. A.; Berry, D. J., Journal of Bone and Joint Surgery-American Volume 97A, 1386 2015.
2. Affatato, S.; Ruggiero, A., Appl. Sci.-Basel 10, 12 2020.
3. Stea, S.; Bordini, B.; De Clerico, M.; Petropulacos, K.; Toni, A., International Orthopaedics 33, 339 2009.
4. Sullivan, S. J. L.; Topoleski, L. D. T., Jom 67, 2502 2015.
5. Zhang, D. M.; Liu, H. T.; Wang, J. M.; Sheng, C. X.; Li, Z. X., Journal of Nanoscience and Nanotechnology 18, 6805 2018.
6. Lu, H.; Ren, S.; Li, X.; Guo, J.; Dong, G.; Li, J.; Gao, L., Journal of Biomaterials Science-Polymer Edition 29, 1331 2018.
7. Kobayashi, M.; Koide, T.; Hyon, S.-H., Journal of the Mechanical Behavior of Biomedical Materials 38, 33 2014.
8. Liu, G.; Cai, M.; Zhou, F.; Liu, W., Journal of Physical Chemistry B 118, 4920 2014.
9. Liu, G.; Liu, Z.; Li, N.; Wang, X.; Zhou, F.; Liu, W., Acs Applied Materials & Interfaces 6, 20452 2014.
10. Ann, K. Y.; Pack, S. W.; Hwang, J. P.; Song, H. W.; Kim, S. H., Construction and Building Materials 24, 1494 2010.
11. Gu, Z.; Huang, B.; Li, Y.; Tian, M.; Li, L.; Yu, X., Materials Science & Engineering C-Materials for Biological Applications 61, 526 2016.
12. Galetz, M. C.; Fleischmann, E. W.; Konrad, C. H.; Schuetz, A.; Glatzel, U., Journal of Biomedical Materials Research Part B-Applied Biomaterials 93B, 244 2010.
13. Scholes, S. C.; Unsworth, A., Journal of Materials Science-Materials in Medicine 20, 163 2009.
14. Liu, H. T.; Ge, S. R.; Cao, S. F.; Wang, S. B., Wear 271, 647 2011.
15. Mishina, H.; Kojima, M., Wear 265, 655 2008.
16. Crockett, R.; Roba, M.; Naka, M.; Gasser, B.; Delfosse, D.; Frauchiger, V.; Spencer, N. D., Journal of Biomedical Materials Research Part A 89A, 1011 2009.
17. Lu, H.; Ren, S.; Guo, J.; Li, Y.; Li, J.; Dong, G., Materials Science & Engineering C-Materials for Biological Applications 78, 239 2017.

18. Ye, E.; Chee, P. L.; Prasad, A.; Fang, X.; Owh, C.; Yeo, V. J. J.; Loh, X. J., Materials Today 17, 194 2014.
19. Deng, W.; Yamaguchi, H.; Takashima, Y.; Harada, A., Chemistry-an Asian Journal 3, 687 2008.
20. Hoare, T. R.; Kohane, D. S., Polymer 49, 1993 2008.
21. Lu, G.; Yan, Q.; Su, X.; Liu, Z.; Ge, C., Progress in Chemistry 19, 485 2007.
22. Feng, Z.; Hu, F.; Lv, L.; Gao, L.; Lu, H., RSC Advances 11, 25530 2021.
23. Chen, K.; Liu, J. L.; Yang, X. H.; Zhang, D. K., Materials Science & Engineering C-Materials for Biological Applications 78, 520 2017.
24. Wu, G.; Zhang, W. G.; Wang, C. T., Journal of Wuhan University of Technology-Materials Science Edition 23, 46 2008.
25. Zhao, X. J.; Zhang, W. L.; Zhou, Z. Q., Colloids and Surfaces B-Biointerfaces 123, 493 2014.
26. Duan, H.; Liu, X.; Liu, C.; Han, T.; Lan, X.; Jiang, Y., Journal of Nanoscience and Nanotechnology 12, 2326 2012.
27. Mou, Z.; Wang, B.; Lu, H.; Dai, S.; Huang, Z., Carbon 154, 301 2019.
28. Guo, J. D.; Mei, T. J.; Li, Y.; Hafezi, M.; Lu, H. L.; Li, J. H.; Dong, G. N., Journal of Biomaterials Science-Polymer Edition 29, 1549 2018.
29. Wang, Y.; Sun, M. X.; Fang, Y. L.; Sun, S. F.; He, J., Journal of Materials Science 51, 779 2016.
30. Song, J.; Li, J.; Guo, Z.; Liu, W.; Ma, Q.; Feng, F.; Dong, C., Rsc Advances 7, 12827 2017.
31. Zhang, S.; Hu, F.; Li, J.; Lv, L.; Lu, H., Advances in Materials Science and Engineering 20212021.
32. Zhao, L.; Ren, Z.; Liu, X.; Ling, Q.; Li, Z.; Gu, H., Acs Applied Materials & Interfaces 13, 11344 2021.
33. Alhazime, A. A., Journal of Inorganic and Organometallic Polymers and Materials 30, 4459 2020.
34. Ding, A.; Zhou, Y.; Chen, P.; Nie, W., Colloid and Polymer Science 295, 1609 2017.
35. Mageswari, S.; Dhivya, L.; Palanivel, B.; Murugan, R., Journal of Alloys and Compounds 545, 41 2012.
36. Saini, I.; Sharma, A.; Dhiman, R.; Aggarwal, S.; Ram, S.; Sharma, P. K., Journal of Alloys and Compounds 714, 172 2017.
37. Massoumi, B.; Jafarpour, P.; Jaymand, M.; Entezami, A. A., Polymer International 64, 689 2015.
38. Huang, K.; Yu, H.; Xie, M.; Liu, S.; Wu, F., Rsc Advances 9, 10599 2019.
39. Wang, H.; Fang, P.; Chen, Z.; Wang, S., Applied Surface Science 253, 8495 2007.
40. Falqi, F. H.; Bin-Dahman, O. A.; Hussain, M.; Al-Harthi, M. A., International Journal of Polymer Science 20182018.
41. Zhang, M.; Na, Y.; Jiang, Z. H., Chemical Journal of Chinese Universities-Chinese 26, 170 2005.
42. Selvi, J.; Mahalakshmi, S.; Parthasarathy, V., Journal of Inorganic and Organometallic Polymers and Materials 27, 1918 2017.
43. Aziz, S. B.; Rasheed, M. A.; Saeed, S. R.; Abdullah, O. G., International Journal of Electrochemical Science 12, 3263 2017.
44. Ghorpade, V. S.; Dias, R. J.; Mali, K. K.; Mulla, S. I., Journal of Drug Delivery Science and Technology 52, 421 2019.